

The Origin of the LCST on the Liquid–Liquid Equilibrium of Thiophene with Ionic Liquids

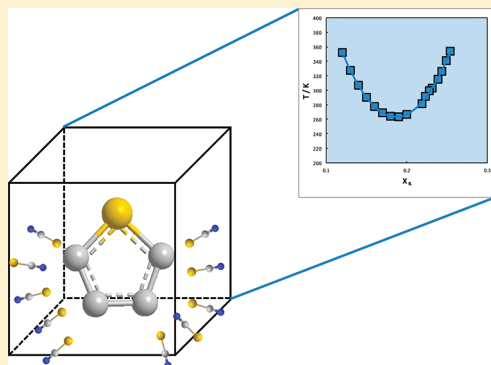
Marta L. S. Batista,[†] Luciana I. N. Tomé,[†] Catarina M. S. S. Neves,[†] Eugénio M. Rocha,[‡] José R. B. Gomes,[†] and João A. P. Coutinho*,[†]

[†]Centre for Research in Ceramics and Composite Materials, CICECO, Departamento de Química, Universidade de Aveiro, 3810-193 Aveiro, Portugal

[‡]Center for Research and Development in Mathematics and Applications, CIDMA, Departamento de Matemática, Universidade de Aveiro, 3810-193 Aveiro, Portugal

Supporting Information

ABSTRACT: Mixtures of thiophene with two ionic liquids, namely, $[C_4C_1im][SCN]$ and $[C_4C_1im][NTf_2]$, were chosen as prototypes of systems presenting lower critical solution temperature (LCST) and upper critical solution temperature (UCST) behavior, respectively. This distinct behavior is due to different interactions between the constituting species which are investigated here by means of experimental and computational studies. Experimentally, density measurements were conducted to assess the excess molar volumes and 1H and ^{13}C NMR spectroscopies were used to obtain the corresponding nuclear chemical shifts with respect to those measured for the pure ionic liquids. Computationally, molecular dynamics simulations were performed to analyze the radial distribution neighborhoods of each species. Negative values of excess molar volumes and strong positive chemical shift deviations for $[C_4C_1im][SCN]$ systems, along with results obtained from MD simulations, allowed the identification of specific interactions between $[SCN]^-$ anion and the molecular solvent (thiophene), which are not observed for $[NTf_2]^-$. It is suggested that these specific $[SCN]^-$ –thiophene interactions are responsible for the LCST behavior observed for mixtures of thiophene with ionic liquids.



INTRODUCTION

Ionic liquids (ILs) are a novel class of salts possessing unique physical and chemical properties, which have been in recent years the focus of great interest for both academic and industrial researchers. They are usually composed by a large asymmetric organic cation and by an anion that can be organic or inorganic. The intricate polar/apolar structure of these species makes their crystallization difficult and minimizes the cation–anion interaction conferring the ILs unique properties, such as a wide liquid temperature range, negligible vapor pressure, high thermal and chemical stabilities, good solvating capacity for both organic and inorganic compounds, and, among others, the ability to tune their properties for specific applications, through innumerable combinations between their ions.^{1,2} These properties make ILs an excellent choice to replace common molecular organic solvents in several applications, namely, extractive solvents in the petrochemical industry for aromatic–aliphatic separations^{3,4} and in the desulfurization of refined products.^{5–7}

The reduction of the sulfur content in fuels has been a major worldwide concern during the past decade.^{6,8,9} The most common desulfurization process is the hydrodesulfurization (HDS), that uses catalysts based on CoMo and NiMo, and high temperatures (300–400 °C) and pressures (20–100 bar of H₂). These operation conditions are costly and have the

disadvantage of removing aliphatic compounds, along with the sulfur ones, and which are important for fuel performance. Alternative processes have been studied to replace or complement HDS such as the oxidative desulfurization, reactive adsorption, biodesulfurization, membranes, and extractive desulfurization which is an attractive process due to its mild and clean conditions, and efficiency.^{5,7,8,10,11} Several ILs have been studied for evaluation of their performance to remove sulfur compounds such as imidazolium^{12–19} and pyridinium-based^{20,21} and also Lewis and Brønsted acidic ILs or oxidative ILs.^{14,22–25}

While measuring the binary^{1,2,26} and ternary^{5,6,11,27} phase diagrams, required to evaluate the capacity of ILs to be used in the extractive desulfurization, it was observed that systems of ILs and thiophene present different types of liquid–liquid equilibrium behavior, which mainly depends on the IL anion. In most cases, these systems display the most common upper critical solution temperature (UCST) behavior, with their mutual miscibilities increasing with a temperature increase, while some others display a lower critical solution temperature (LCST).^{1,2} Examples of these behaviors are presented in Figure 1 for thiophene combined with $[C_4C_1im][NTf_2]$ (UCST) or

Received: April 3, 2012

Published: May 2, 2012

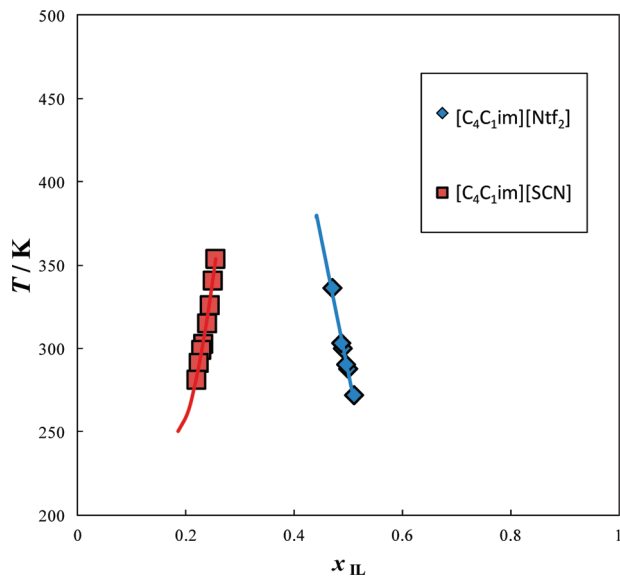


Figure 1. Phase diagram of temperature as a function of mole fraction of $[\text{C}_4\text{C}_1\text{im}][\text{SCN}]^1$ and $[\text{C}_4\text{C}_1\text{im}][\text{NTf}_2]^{28}$. Lines are guides to the eye.

$[\text{C}_4\text{C}_1\text{im}][\text{SCN}]$ (LCST).^{1,28} The molecular structures of both ILs, $[\text{C}_4\text{C}_1\text{im}][\text{NTf}_2]$ and $[\text{C}_4\text{C}_1\text{im}][\text{SCN}]$, as well as thiophene are displayed in Figure S.1 in the Supporting Information.

Given the impact that the phase behavior has on the design of extraction processes, and the importance of understanding the liquid–liquid demixing to optimize the design of ILs to be used in desulfurization approaches, the differences in the interactions between ILs and thiophene, that generate the two types of phase diagrams observed, are here investigated. For that purpose, the systems of thiophene with $[\text{C}_4\text{C}_1\text{im}][\text{NTf}_2]$ and $[\text{C}_4\text{C}_1\text{im}][\text{SCN}]$ were studied using ^1H and ^{13}C NMR spectroscopy, excess volume measurements, and computer simulations. By analyzing the chemical shift deviation ($\Delta\delta$) and the excess molar volumes (V^E), as well as the calculated radial distribution functions, a comprehensive picture of the molecular interactions between the ILs and thiophene was drawn, which explains the formation of the two types of phase diagrams (UCST and LCST).

■ EXPERIMENTAL SECTION

Materials. Thiophene was supplied by Acros with a purity of 99.5 wt %. The ILs used in this work were supplied by IoLiTec and comprise 1-butyl-3-methylimidazolium bis(trifluoromethylsulfonyl)imide, $[\text{C}_4\text{C}_1\text{im}][\text{NTf}_2]$, with mass fraction purity >99 wt %, and 1-butyl-3-methylimidazolium thiocyanate, $[\text{C}_4\text{C}_1\text{im}][\text{SCN}]$, with mass fraction purity >98 wt %. Their purities were further confirmed by ^1H , ^{13}C , and ^{19}F (for the fluorinated fluid) NMR. In order to reduce the amount of volatile impurities, all samples were dried for at least 48 h under vacuum (10^{-5} Pa) and at room temperature before use. After the drying procedure, the water content in the samples, measured by Karl–Fischer titration, was found to be 89 and 354 ppm for $[\text{C}_4\text{C}_1\text{im}][\text{NTf}_2]$ and $[\text{C}_4\text{C}_1\text{im}][\text{SCN}]$, respectively.

Experimental Procedure. All mixtures of the ILs with thiophene were prepared gravimetrically with an uncertainty of $\pm 10^{-4}$ g. In order to homogenize the mixtures, they were constantly stirred for at least 24 h at room temperature.

Density measurements were performed at atmospheric pressure and in a temperature range from 298.15 to 348.15 K, using

an automated SVM 3000 Anton Paar rotational Stabinger viscometer-densimeter. The SVM 3000 Anton Paar rotational Stabinger viscometer-densimeter uses Peltier elements for fast and efficient thermostabilization. This equipment has been previously tested and used by us^{29,30} for the density measurement of ionic liquids. The uncertainty in temperature is within ± 0.02 K, while the absolute uncertainty for density is $\pm 5 \times 10^{-4}$ g·cm⁻³.

For the NMR analysis, a stem coaxial capillary tube was used with acetone- d_6 that was inserted into 5 mm NMR tubes with the different mixtures composed of IL and thiophene. The ^1H and ^{13}C were recorded using a Bruker Avance 300 spectrometer operating at 300.13 and 75.47 MHz, respectively.

■ COMPUTATIONAL DETAILS

The interaction between ILs and thiophene was investigated by molecular dynamics (MD) simulation using the GROMACS 4.5.4 molecular dynamics package.³¹ These simulations were carried out in the constant temperature and constant pressure (NPT) ensemble. Constant temperature (298.15 K) was maintained by using the Nosé–Hoover^{32,33} thermostat, while the pressure (1 bar) was maintained by using the Parrinello–Rahman³⁴ barostat. All systems (each one considering 80 pairs of IL ions and 40 molecules of thiophene) were prepared by randomly placing all species in the simulation boxes. In each of these simulations, the equations of motion were integrated with the Verlet–Leapfrog³⁵ algorithm and a time step of 2 fs. A 10 000 step energy minimization was performed, and the systems were equilibrated (at least 150 000 steps). Further, quite long simulations were carried out, with 25 000 000 steps for $[\text{C}_4\text{C}_1\text{im}][\text{SCN}]$ with thiophene and 50 000 000 steps for $[\text{C}_4\text{C}_1\text{im}][\text{NTf}_2]$ with thiophene (50 ns). The intermolecular interaction energy between pairs of neighboring atoms was calculated using the Lennard-Jones potential to describe dispersion/repulsion forces, and the point-charge Coulomb potential was used for electrostatic interactions. Long-range electrostatic interactions were accounted for using the particle-mesh Ewald³⁶ method with a cutoff of 1.0 nm for the real-space part of the interactions. A cutoff radius of 1.2 nm was used for the Lennard-Jones potential, and long-range dispersion interactions were added to both energy and pressure. Rigid constraints were enforced on all bond lengths.

All-atom force fields for $[\text{C}_4\text{C}_1\text{im}][\text{NTf}_2]$ were obtained from the works of Cadena and Maginn³⁷ and of Canongia Lopes and Pádua³⁸ for the cation and for the anion, respectively, as in the work of Tomé et al.³⁹ The charges for the cation and the anion were recalculated with the CHelpG scheme using an optimized geometry for the $\text{C}_4\text{C}_1\text{im}-\text{NTf}_2$ dimer in the gas phase.³⁹ The calculations considered the B3LYP/6-311+G(d) approach as included in the Gaussian 03 code,⁴⁰ i.e., using the same computational strategy employed by Morrow and Maginn for the $[\text{C}_4\text{C}_1\text{im}][\text{PF}_6]$ ionic liquid.⁴¹ The total charges on the cation and anion are +0.797 and −0.797 au, respectively. The estimation of partial charges for an IL from calculations of an ion pair in a vacuum can be a problematic treatment, and this issue has been addressed and discussed in other works.^{42,43} Nevertheless, it has been demonstrated that models with total charges on each ion in the range ± 0.7 –0.8 yield a better description of both structural and (most noticeably) dynamic properties of ionic liquids.^{43–45} Furthermore, we have also performed calculations considering a pair of ions surrounded by other IL ions and no significant differences were found in the results obtained. The full set of atomic charges is supplied as

Supporting Information (Tables S.1–S.3). The calculated density and enthalpy of vaporization for $[C_4C_1im][NTf_2]$ are 1486 kg/m³ and 131.74 kJ/mol, respectively, which compare well with the range of experimental results, i.e., [1429; 1437.4] kg/m³^{46,47} and 134–155 kJ/mol,⁴⁸ respectively. In the case of $[C_4C_1im][SCN]$, we have used the all-atom force field from the work of Cadena and Maginn³⁷ for the cation and we have adapted standard Gromos potential parameters for the anion (additional details given in Tables S.4–S.7 supplied as Supporting Information). The CHelpG total charges on the cation and anion are +0.791 and -0.791 au, respectively. These values were also calculated using a B3LYP/6-311+G(d) optimized geometry (minimum energy from several initial configurations) for the C_4C_1im -SCN dimer in the gas phase. It was quite encouraging to see that the charges above are close to those computed for the central cation/anion pair in clusters containing several $[C_4C_1im][SCN]$ pairs; for instance, the mean values calculated for the central dimer in different clusters containing 13 C_4C_1im -SCN pairs are $+0.804 \pm 0.020$ and -0.804 ± 0.020 au for the cation and the anion, respectively. The calculated density and enthalpy of vaporization for $[C_4C_1im][SCN]$ are 1082 kg/m³ and 123.0 kJ/mol, respectively. Very encouraging, these results compare well with the range of experimental results for density and enthalpy of vaporization, i.e., [1070; 1069.8] kg/m³^{47,49} and 114.5–148 kJ/mol,⁵⁰ respectively. The spatial distribution functions (SDF) were calculated using a bin width of 0.05 nm.

RESULTS AND DISCUSSION

Excess Volumes (V^E). This property describes the deviation of the mixture molar volume from the ideal molar volume. The excess molar volume is estimated from the measured densities as described in eq 1

$$V^E = \sum x_i M_i \left(\frac{1}{\rho_{\text{mixt}}} - \frac{1}{\rho_i} \right) \quad (1)$$

where x_i , M_i , and ρ_i are the molar fraction, molar mass, and density for each component that composes the binary system and ρ_{mixt} is the density of the mixture.

V^E data can be used to obtain information on the strength/type of interactions between components in a given mixture. Negative values of V^E usually indicate strong and favorable interactions, while positive values of V^E indicate nonfavorable interactions.

Results for the excess molar volumes of the mixtures composed of thiophene with $[C_4C_1im][NTf_2]$ or $[C_4C_1im][SCN]$, within their mutual miscibility range, are presented in Figures 2 and 3, respectively.

Both figures represent data for two temperatures, and independently of the temperature chosen, there is an opposite behavior for mixtures constituted by thiophene and one of the ILs considered. In Figure 2, it is shown that the $[C_4C_1im][NTf_2]$ -containing system presents large and positive excess molar volumes when mixed with thiophene. This pattern is indeed indicative of nonspecific and nonfavorable interactions between the IL ions and thiophene. On the contrary, in the case of the $[C_4C_1im][SCN]$ mixtures with thiophene (Figure 3), negative excess molar volumes are observed in the entire range of compositions. This trend suggests and supports the existence of some sort of specific interaction among the ILs and the molecular species. These findings are in good agreement with the phase diagrams presented in Figure 1.

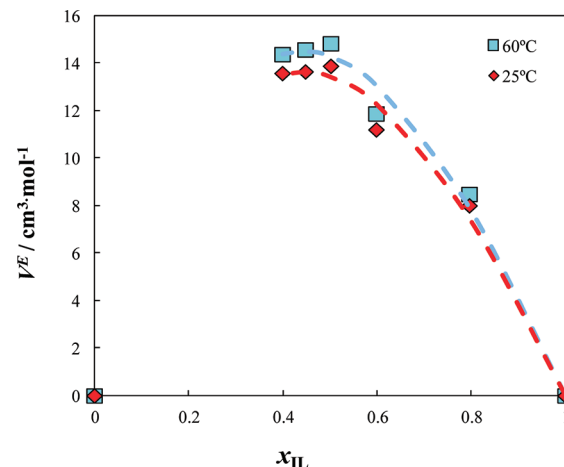


Figure 2. Excess volumes as a function of mole fraction of $[C_4C_1im][NTf_2]$, at different temperatures. Lines are guides to the eye.

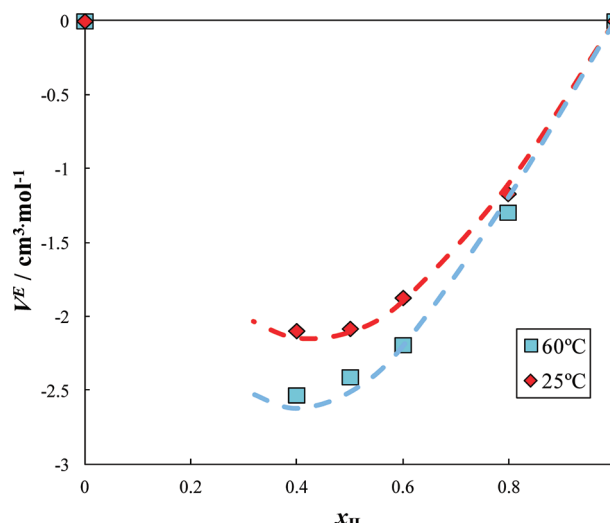


Figure 3. Excess volumes as a function of mole fraction of $[C_4C_1im][SCN]$, at different temperatures. Lines are guides to the eye.

Chemical Shift Deviations ($\Delta\delta$). ¹H and ¹³C NMR spectroscopy are widely used to identify the structure of compounds through differentiation of the atomic neighborhood of protons and carbons, but they may also be a powerful technique to identify favorable or nonfavorable interactions among different compounds.^{51,52} Each type of proton or carbon in a different structural/chemical environment has a characteristic chemical shift (δ_i), represented by the peaks of a NMR spectrum. These peaks are shifted to higher or lower chemical shifts depending on the type of interactions that a given carbon and/or proton suffer in a mixture. The chemical shift deviations ($\Delta\delta$) are defined by the following equation

$$\Delta\delta = \delta_{\text{mixt}} - \delta_{\text{IL}} \quad (2)$$

where, in this work, δ_{mixt} is the ¹H/¹³C chemical shift of the IL in mixtures with thiophene and δ_{IL} is related to the chemical shift of the pure IL. In general, positive $\Delta\delta$ identify favorable interactions involving those nuclei, while negative $\Delta\delta$ values identify atoms with a lower propensity to interact. Finally, protons or carbons with $\Delta\delta$ values close to zero are not involved in significant and additional interactions.

Figures 4 and 5 represent the ^1H and ^{13}C chemical shift deviations ($\Delta\delta$) for mixtures composed of $[\text{C}_4\text{C}_1\text{im}][\text{SCN}]$

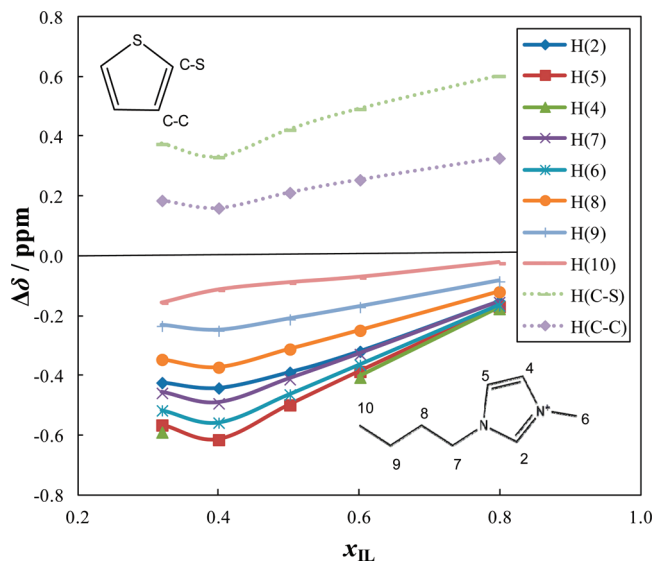


Figure 4. ^1H NMR chemical shift deviations for $[\text{C}_4\text{C}_1\text{im}][\text{SCN}]$ in the mixture with thiophene. The dotted lines represent the hydrogen chemical shift deviations for thiophene and full lines for the cation $[\text{C}_4\text{C}_1\text{im}]^+$.

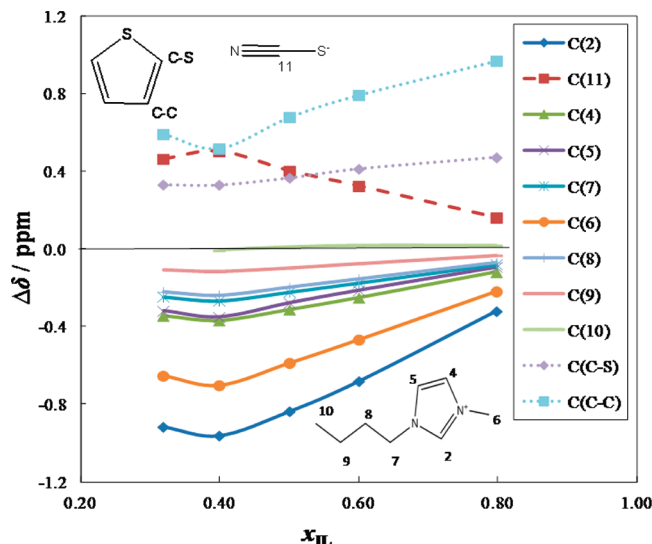


Figure 5. ^{13}C NMR chemical shift deviations for $[\text{C}_4\text{C}_1\text{im}][\text{SCN}]$ in the mixture with thiophene. The dotted lines represent the carbon chemical shift deviations for thiophene, full lines for the cation $[\text{C}_4\text{C}_1\text{im}]^+$, and dashed lines for the anion $[\text{SCN}]^-$.

and thiophene, whereas Figures 6 and 7 show the ^1H and ^{13}C chemical shift deviations ($\Delta\delta$) for mixtures of $[\text{C}_4\text{C}_1\text{im}][\text{NTf}_2]$ and thiophene. Detailed information concerning the individual chemical shifts is presented in Tables S.8–S.15 in the Supporting Information.

For the two evaluated mixtures, only the proton chemical shifts of thiophene present positive chemical shift deviations. Albeit thiophene displays favorable interactions with both ILs, these are particularly strong in the presence of $[\text{C}_4\text{C}_1\text{im}][\text{SCN}]$. In both ILs, the protons of the cation present negative deviations which suggest that they are not actively interacting

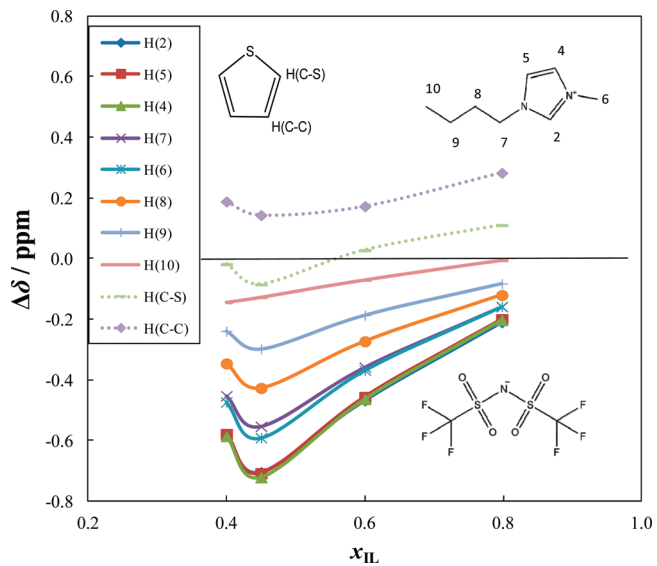


Figure 6. ^1H NMR chemical shift deviations for $[\text{C}_4\text{C}_1\text{im}][\text{NTf}_2]$ in the mixture with thiophene. The dotted lines represent the hydrogen chemical shift deviations for thiophene and full lines for the cation $[\text{C}_4\text{C}_1\text{im}]^+$.

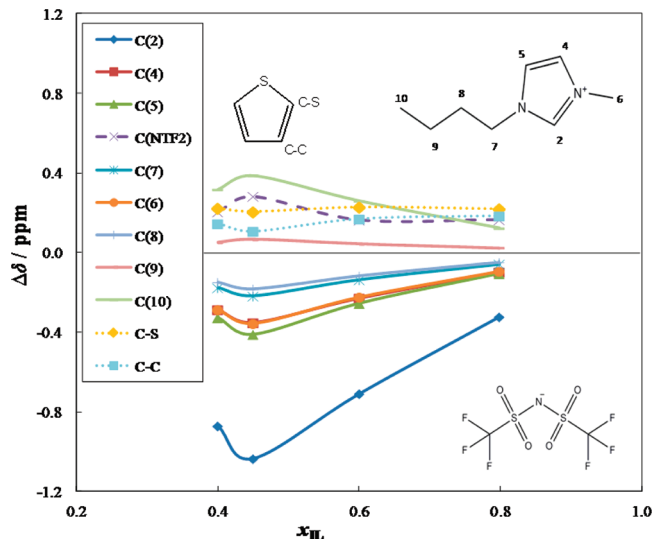


Figure 7. ^{13}C NMR chemical shift deviations for $[\text{C}_4\text{C}_1\text{im}][\text{NTf}_2]$ in the mixture with thiophene. The dotted lines represent the carbon chemical shift deviations for thiophene, full lines for the cation $[\text{C}_4\text{C}_1\text{im}]^+$, and dashed lines for the anion $[\text{NTf}_2]^-$.

with thiophene. Moreover, these nonfavorable interactions observed at the ^1H NMR are more evident with $[\text{C}_4\text{C}_1\text{im}][\text{NTf}_2]$. Therefore, there is clear evidence that the favorable interactions of thiophene occur with the IL anions. This is confirmed by the ^{13}C chemical shift deviations presented in Figures 5 and 7. Again strong positive chemical shift deviations for the aromatic thiophene carbons are observed with the $[\text{C}_4\text{C}_1\text{im}][\text{SCN}]$ -containing systems, along with strong deviations in the $[\text{SCN}]^-$ carbon, both increasing with the content of the other species (with the exception of the carbon atom of the anion, which decreases). Although some favorable interactions are also observed with $[\text{NTf}_2]^-$ carbon atoms, these seem to be less significant taking into account the magnitude of the chemical shift deviations. Therefore, the NMR data clearly suggest that favorable interactions between thiophene and each

IL exist, although they are more significant for the $[SCN]^-$ -based fluid.

Molecular Dynamics Simulations. In this type of computer simulations involving a large number of atoms, the radial distribution function, $g(x)$ or RDF, can be employed to describe the structural organization of a system. This function gives the probability of finding a particle at the distance r , from another particle (considered as the reference particle) and will be used here to aid the interpretation of the experimental results. The $g(x)$ values provide a quantitative description of enhancement (values larger than 1) or depletion (values smaller than 1) of densities of atoms or groups of atoms around a selected moiety with respect to bulk values. The calculated radial distribution functions are depicted in Figures 8–11, while peak maxima are given in Tables S.16–S.19 (Supporting Information).

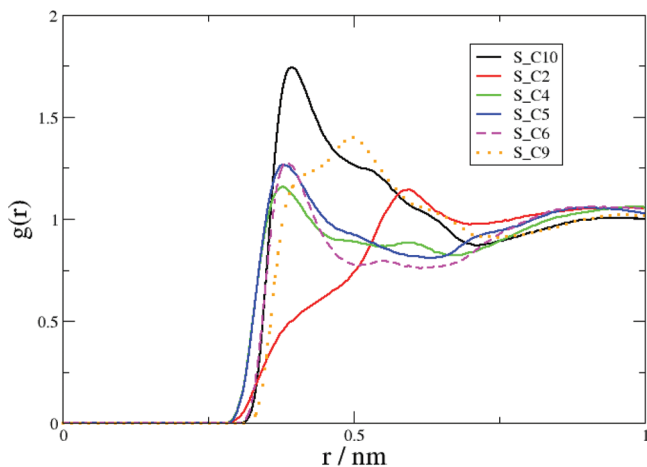


Figure 8. Radial distribution functions of selected carbon atoms of $[C_4C_1\text{im}]^+$ around the S atom of thiophene in the system $[C_4C_1\text{im}][\text{SCN}] + \text{thiophene}$.

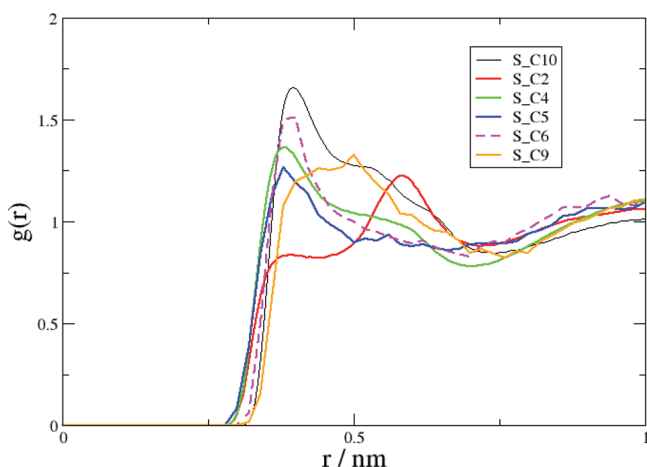


Figure 9. Radial distribution functions of selected carbon atoms of $[C_4C_1\text{im}]^+$ around the S atom of thiophene in the system $[C_4C_1\text{im}][\text{NTf}_2] + \text{thiophene}$.

Cation–Thiophene Interactions. For the cation of $[C_4C_1\text{im}][\text{SCN}]$, there is a higher intensity peak for the atom C10, the carbon at the alkyl chain extremity, especially when considering the atom of sulfur of thiocyanate (Figure 8). However, the atoms at the ring of the imidazolium cation (except the C2) as well as the carbon C6 from the methyl

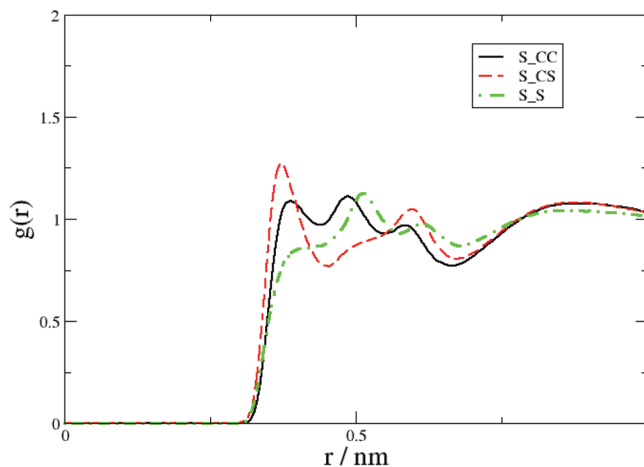


Figure 10. Radial distribution functions of thiophene atoms around the S atom of $[\text{SCN}]^-$ in the system $[C_4C_1\text{im}][\text{SCN}] + \text{thiophene}$.

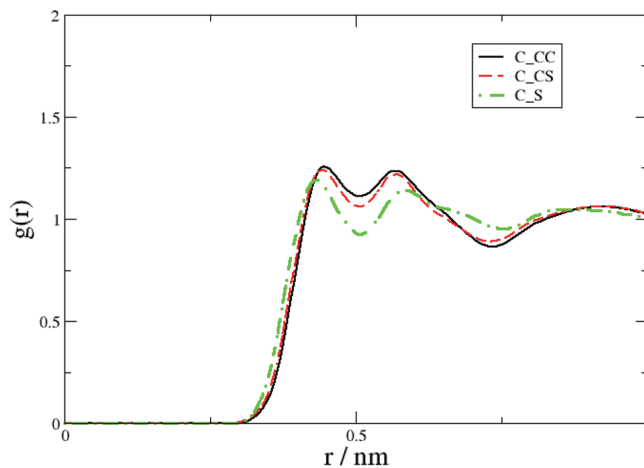
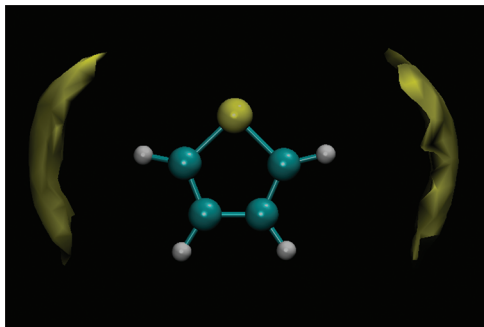


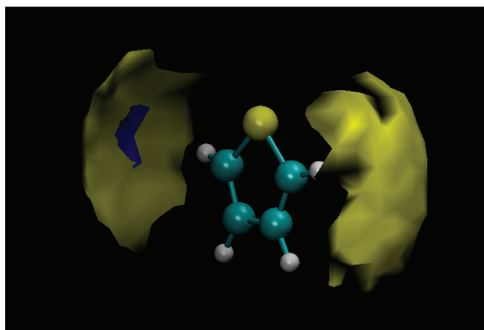
Figure 11. Radial distribution functions of thiophene atoms around the C1 atom of $[\text{NTf}_2]^-$ in the system $[C_4C_1\text{im}][\text{NTf}_2] + \text{thiophene}$.

group show also significant interactions with thiophene. Since both ILs are composed by the same cation, it is not surprising to see that, in the case of $[C_4C_1\text{im}][\text{NTf}_2]$, Figure 9, the radial distribution functions are similar to those calculated for $[C_4C_1\text{im}][\text{SCN}]$; i.e., the interactions involve the same atoms. However, in the case of $[C_4C_1\text{im}][\text{NTf}_2]$, the intensities of the S–C(cation) peaks are higher than those observed with $[C_4C_1\text{im}][\text{SCN}]$. Thus, these intensities suggest that the cation interactions with thiophene are dominant in the former IL.

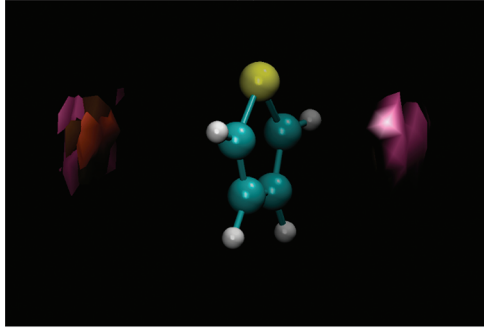
Anion–Thiophene Interactions. The RDFs calculated for the interactions involving the $[\text{SCN}]^-$ and $[\text{NTf}_2]^-$ anions and thiophene are displayed in Figures 10 and 11, respectively. Figure 10 shows that the sulfur atom of thiocyanate has a higher probability to surround the carbon atoms of thiophene (the CS and CC carbons) than to surround the sulfur atom, with peak intensity maxima of 1.26 for CS and 1.08/1.11 double peak corresponding to CC atoms. The RDFs calculated for the C and N atoms of $[\text{SCN}]^-$ do not present visible peak intensity maxima (Figure S.2 in the Supporting Information), suggesting that S atoms are pointing toward the thiophene carbon atoms while the former atoms are rotating in a conical shape oriented outward from the thiophene ring. For systems composed of $[C_4C_1\text{im}][\text{NTf}_2]$ and thiophene, the RDFs calculated for atoms of $[\text{NTf}_2]^-$ and thiophene show peaks



(a)



(b)

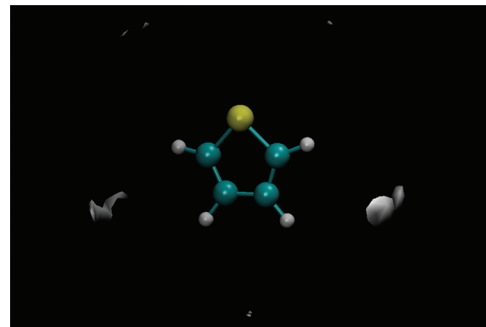


(c)

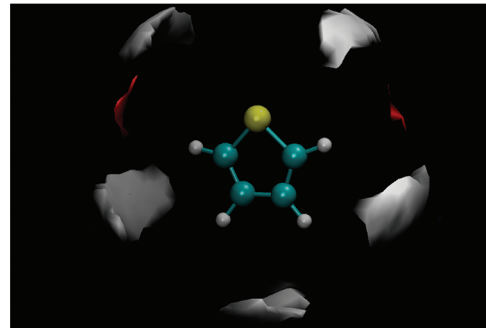
Figure 12. Spatial distribution functions (SDF) for $[\text{SCN}]^-$ (a, b) and $[\text{C}_4\text{C}_1\text{im}]^+$ (c) around thiophene from MD simulation of the $[\text{C}_4\text{C}_1\text{im}][\text{SCN}] + \text{thiophene}$ mixture. Yellow and blue regions stand for SDF (isovalue = 25) of S and N atoms from the IL anion, respectively. Mauve, orange, and brown regions stand for SDF (isovalue = 32) C10, C4, and C6 atoms of the IL cation, respectively.

that occur at large distances, with $g(x)$ values being close to or lower than unity (Figures 11 and S.3 in the Supporting Information). Nevertheless, in the case of the carbon from the anion (note that the anion $[\text{NTf}_2]^-$ is here considered to be a symmetric structure, similar to thiophene), in Figure 11, there is significant interaction between this atom and thiophene constituting atoms which is represented by a double peak (with very similar RDF shapes for the three different atomic species of thiophene). In summary, the RDFs show a more specific orientation of the anion $[\text{SCN}]^-$ around the thiophene moiety, with a preferable orientation toward CS and CC atoms of thiophene, suggesting more favorable interactions with the latter atoms than with the sulfur atom of thiophene. These specific orientations are not evident in the case of the $[\text{NTf}_2]^-$ anion for which similar RDFs were obtained for all the interactions with thiophene.

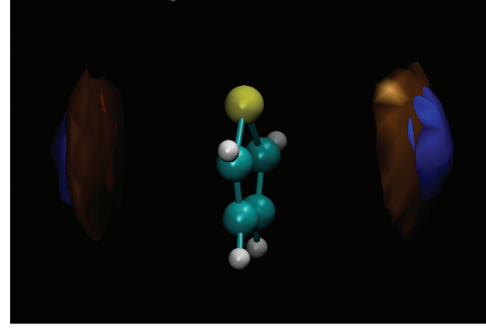
Final Remarks. In summary, negative values of V^E and positive ^{13}C chemical shift deviations revealed the presence of favorable and stronger interactions of thiophene with the



(a)



(b)



(c)

Figure 13. Spatial distribution functions (SDF) for $[\text{NTf}_2]^-$ (a, b) and $[\text{C}_4\text{C}_1\text{im}]^+$ (c) around thiophene from MD simulation of the $[\text{C}_4\text{C}_1\text{im}][\text{NTf}_2] + \text{thiophene}$ mixture. White and red regions stand for SDF (isovalue are 25 in a and 20 in b, respectively) of C and O atoms from the IL anion, respectively. Blue, orange, and brown regions stand for SDF (isovalue = 32) N3, C4, and C6 atoms of the IL cation, respectively.

$[\text{SCN}]^-$ anion. MD simulations provided a reinforcement to the results obtained experimentally, since it was possible to identify a specific interaction between $[\text{SCN}]^-$ and thiophene through a well-defined spatial orientation which is thus responsible for the LCST behavior. For the system composed of $[\text{C}_4\text{C}_1\text{im}][\text{NTf}_2]$ and thiophene, the common UCST behavior is observed—behavior typical of systems with weaker and/or nonfavorable interactions. The positive values of V^E and the dispersion forces acting between the thiophene and the terminal groups of the alkyl chains of the cations are in good agreement with this type of phase diagram.

The results here reported confirm the suggestion of Revelli et al.⁹ which posed that a specific interaction is present in the binary system $[\text{C}_4\text{C}_1\text{im}][\text{SCN}]$ –thiophene; however, the molecular picture gathered from this work is completely different from that initially proposed. They suggested that four thiophene molecules in a pseudo-tetrahedron spatial orientation were surrounding the $[\text{SCN}]^-$ anion with its sulfur atom

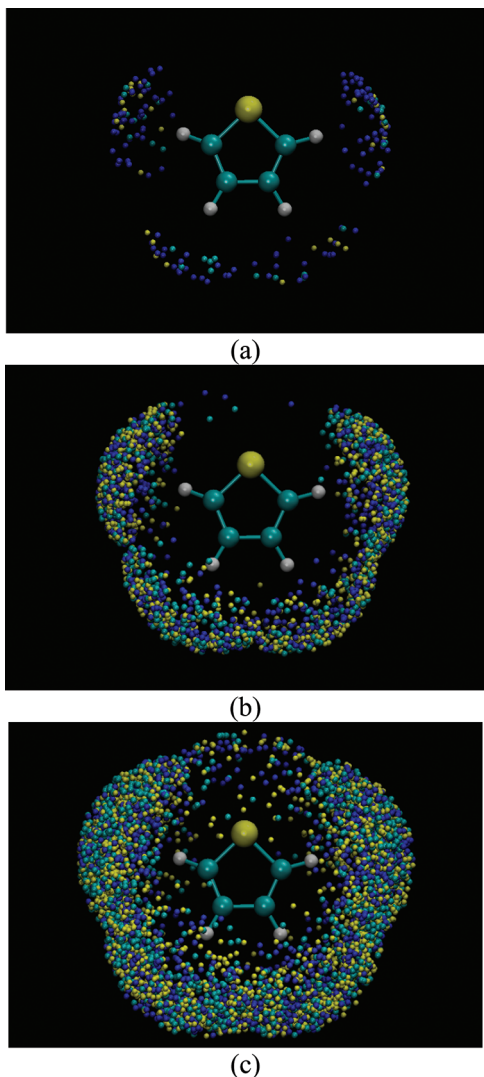


Figure 14. Atomic hits for SCN-constituting atoms at (a) 2.5 Å, (b) 3.0 Å, and (c) 3.5 Å around thiophene from MD simulation of the $[C_4C_1\text{im}][\text{SCN}]$ + thiophene mixture. Yellow, blue, cyan, and white spheres stand for sulfur, nitrogen, carbon, and hydrogen atoms, respectively.

pointed toward the anion. This suggestion is not compatible with the results reported here. In fact, both the NMR and MD results presented and discussed above show that the anion $[\text{SCN}]^-$ preferentially surrounds the CS and CC carbons of thiophene, as shown in Figures 12–14. As can be seen from the spatial distribution functions (SDFs), there is clear preference for $[\text{SCN}]^-$ constituting atoms to be located closer to CC and CS atoms than to the S atom of thiophene (Figure 12), while in the case of the $[\text{NTf}_2]^-$ species signs of preferential orientation are unseen (Figure 13). The same figures show that the location of the cation, which is the same in the two ILs considered in this work, is the same for mixtures of thiophene with both ILs.

CONCLUSIONS

The different liquid–liquid equilibrium behaviors of $[C_4C_1\text{im}][\text{SCN}]$ and $[C_4C_1\text{im}][\text{NTf}_2]$ with thiophene were investigated by means of experimental and computational work. For these systems, density measurements and ^1H and ^{13}C NMR spectra were used to estimate the excess molar volumes and chemical shift deviations that, along with molecular dynamics simulations,

were used to understand the molecular basis of the phenomena observed.

Negative values of V^E , as well as strong positive chemical shift deviations for the carbon atom from the anion $[\text{SCN}]^-$ obtained for the $[C_4C_1\text{im}][\text{SCN}]$ systems, showed the presence of strong and specific interactions between the ionic liquid anion and the thiophene protons. The molecular dynamics simulations further supported this view. For $[C_4C_1\text{im}][\text{SCN}]$, it was possible to identify a specific spatial orientation of the sulfur atom of the anion with the thiophene protons which is suggested to be responsible for the LCST behavior. The interactions of thiophene with other ionic liquids, here represented by the $[C_4C_1\text{im}][\text{NTf}_2]$, are of a different nature, being weak and of a dispersive type between the cation alkyl chains and the thiophene, leading to the more common UCST type of liquid–liquid phase diagram.

ASSOCIATED CONTENT

S Supporting Information

Lists of CHelpG atomic charges and Lennard-Jones parameters for the species considered; ^1H and ^{13}C NMR chemical shift deviations for the different systems considered; position and intensities of RDF peak maxima; additional RDFs. This material is available free of charge via the Internet at <http://pubs.acs.org>.

AUTHOR INFORMATION

Corresponding Author

*Phone: +351-234-370200. Fax: +351-234-370084. E-mail: jcoutinho@ua.pt.

Notes

The authors declare no competing financial interest.

ACKNOWLEDGMENTS

The authors acknowledge financial support from FCT-Fundaçao para a Ciéncia e a Tecnologia, for project PEst-C/CTM/LA0011/2011, for Programa Ciéncia 2007, and for the grants SFRH/BPD/44926/2008, SFRH/BD/70641/2010, and SFRH/BD/74551/2010 awarded to L.I.N.T., C.M.S.S.N., and M.L.S.B., respectively.

REFERENCES

- (1) Domańska, U.; Krokowski, M.; Slesinska, K. *J. Chem. Thermodyn.* **2009**, *41*, 1303–1311.
- (2) Marciniak, A.; Karczemna, E. *Fluid Phase Equilib.* **2011**, *307*, 160–165.
- (3) Ferreira, A. R.; Freire, M. G.; Ribeiro, J. C.; Lopes, F. M.; Crespo, J. G.; Coutinho, J. A. P. *Ind. Eng. Chem. Res.* **2011**, *50*, 5279–5294.
- (4) Meindersma, G. W.; Hansmeier, A. R.; de Haan, A. B. *Ind. Eng. Chem. Res.* **2010**, *49*, 7530–7540.
- (5) Francisco, M.; Arce, A.; Soto, A. *Fluid Phase Equilib.* **2010**, *294*, 39–48.
- (6) Kedra-Krolik, K.; Fabrice, M.; Jaubert, J.-N. *Ind. Eng. Chem. Res.* **2011**, *50*, 2296–2306.
- (7) Kulkarni, P. S.; Afonso, C. A. M. *Green Chem.* **2010**, *12*, 1139–1149.
- (8) Anantharaj, R.; Banerjee, T. *Fuel Process. Technol.* **2011**, *92*, 39–52.
- (9) Revelli, A. L.; Mutelet, F.; Jaubert, J. N. *J. Phys. Chem. B* **2010**, *114*, 4600–4608.
- (10) Hansmeier, A. R.; Meindersma, G. W.; de Haan, A. B. *Green Chem.* **2011**, *13*, 1907–1913.
- (11) Kedra-Krolik, K.; Mutelet, F.; Moise, J.-C.; Jaubert, J.-N. *Energy Fuels* **2011**, *25*, 1559–1565.

- (12) Alonso, L.; Arce, A.; Francisco, M.; Rodriguez, O.; Soto, A. *AIChE J.* **2007**, *53*, 3108–3115.
- (13) Alonso, L.; Arce, A.; Francisco, M.; Soto, A. *J. Chem. Thermodyn.* **2008**, *40*, 966–972.
- (14) Bosmann, A.; Datsevich, L.; Jess, A.; Lauter, A.; Schmitz, C.; Wasserscheid, P. *Chem. Commun.* **2001**, 2494–2495.
- (15) Jiang, X.; Nie, Y.; Li, C.; Wang, Z. *Fuel* **2008**, *87*, 79–84.
- (16) Mochizuki, Y.; Sugawara, K. *Energy Fuels* **2008**, *22*, 3303–3307.
- (17) Nie, Y.; Li, C.; Sun, A.; Meng, H.; Wang, Z. *Energy Fuels* **2006**, *20*, 2083–2087.
- (18) Nie, Y.; Li, C.-X.; Wang, Z.-H. *Ind. Eng. Chem. Res.* **2007**, *46*, 5108–5112.
- (19) Zhang, S. G.; Zhang, Z. C. *Green Chem.* **2002**, *4*, 376–379.
- (20) Gao, H.; Luo, M.; Xing, J.; Wu, Y.; Li, Y.; Li, W.; Liu, Q.; Liu, H. *Ind. Eng. Chem. Res.* **2008**, *47*, 8384–8388.
- (21) Holbrey, J. D.; Lopez-Martin, I.; Rothenberg, G.; Seddon, K. R.; Silvero, G.; Zheng, X. *Green Chem.* **2008**, *10*, 87–92.
- (22) Gao, H.; Xing, J.; Li, Y.; Li, W.; Liu, Q.; Liu, H. *Sep. Sci. Technol.* **2009**, *44*, 971–982.
- (23) Huang, C. P.; Chen, B. H.; Zhang, J.; Liu, Z. C.; Li, Y. X. *Energy Fuels* **2004**, *18*, 1862–1864.
- (24) Ko, N. H.; Lee, J. S.; Huh, E. S.; Lee, H.; Jung, K. D.; Kim, H. S.; Cheong, M. *Energy Fuels* **2008**, *22*, 1687–1690.
- (25) Yang, Y. L.; Kou, Y. *Chem. Commun.* **2004**, 226–227.
- (26) Lachwa, J.; Szydlowski, J.; Makowska, A.; Seddon, K. R.; Esperanca, J.; Guedes, H. J. R.; Rebelo, L. P. N. *Green Chem.* **2006**, *8*, 262–267.
- (27) Arce, A.; Earle, M. J.; Rodriguez, H.; Seddon, K. R.; Soto, A. *Green Chem.* **2008**, *10*, 1294–1300.
- (28) Batista, M. L. S.; Neves, C. M. S. S.; Tomé, L. I. N.; Gomes, J. R. B.; Coutinho, J. A. P. *J. Chem. Eng. Data* **2012**, submitted for publication.
- (29) Neves, C. M. S. S.; Batista, M. L. S.; Claudio, A. F. M.; Santos, L. M. N. B. F.; Marrucho, I. M.; Freire, M. G.; Coutinho, J. A. P. *J. Chem. Eng. Data* **2010**, *55*, 5065–5073.
- (30) Neves, C. M. S. S.; Carvalho, P. J.; Freire, M. G.; Coutinho, J. A. P. *J. Chem. Thermodyn.* **2011**, *43*, 948–957.
- (31) Hess, B.; Kutzner, C.; van der Spoel, D.; Lindahl, E. *J. Chem. Theory Comput.* **2008**, *4*, 435–447.
- (32) Hoover, W. G. *Phys. Rev. A* **1985**, *31*, 1695–1697.
- (33) Nose, S. *Mal. Phys.* **1984**, *52*, 255–268.
- (34) Parrinello, M.; Rahman, A. *J. Appl. Phys.* **1981**, *52*, 7182–7190.
- (35) Hockney, R. W.; Goel, S. P.; Eastwood, J. W. *J. Comput. Phys.* **1974**, *14*, 148–158.
- (36) Essmann, U.; Perera, L.; Berkowitz, M. L.; Darden, T.; Lee, H.; Pedersen, L. G. *J. Chem. Phys.* **1995**, *103*, 8577–8593.
- (37) Cadena, C.; Maginn, E. J. *J. Phys. Chem. B* **2006**, *110*, 18026–18039.
- (38) Canongia Lopes, J. N.; Pádua, A. A. H. *J. Phys. Chem. B* **2004**, *108*, 16893.
- (39) Tome, L. I. N.; Jorge, M.; Gomes, J. R. B.; Coutinho, J. A. P. *J. Phys. Chem. B* **2012**, *116*, 1831–1842.
- (40) Frisch, M. J.; Trucks, G. W.; Schlegel, H. B.; Scuseria, G. E.; Robb, M. A.; Cheeseman, J. R.; Montgomery, J. A., Jr.; Vreven, T.; Kudin, K. N.; Burant, J. C.; Millam, J. M.; Iyengar, S. S.; Tomasi, J.; Barone, V.; Mennucci, B.; Cossi, M.; Scalmani, G.; Rega, N.; Petersson, G. A.; Nakatsuji, H.; Hada, M.; Ehara, M.; Toyota, K.; Fukuda, R.; Hasegawa, J.; Ishida, M.; Nakajima, T.; Honda, Y.; Kitao, O.; Nakai, H.; Klene, M.; Li, X.; Knox, J. E.; Hratchian, H. P.; Cross, J. B.; Bakken, V.; Adamo, C.; Jaramillo, J.; Gomperts, R.; Stratmann, R. E.; Yazayev, O.; Austin, A. J.; Cammi, R.; Pomelli, C.; Ochterski, J. W.; Ayala, P. Y.; Morokuma, K.; Voth, G. A.; Salvador, P.; Dannenberg, J. J.; Zakrzewski, V. G.; Dapprich, S.; Daniels, A. D.; Strain, M. C.; Farkas, O.; Malick, D. K.; Rabuck, A. D.; Raghavachari, K.; Foresman, J. B.; Ortiz, J. V.; Cui, Q.; Baboul, A. G.; Clifford, S.; Cioslowski, J.; Stefanov, B. B.; Liu, G.; Liashenko, A.; Piskorz, P.; Komaromi, I.; Martin, R. L.; Fox, D. J.; Keith, T.; Al-Laham, M. A.; Peng, C. Y.; Nanayakkara, A.; Challacombe, M.; Gill, P. M. W.; Johnson, B.; Chen, W.; Wong, M. W.; Gonzalez, C.; Pople, J. A. *Gaussian 03*, revision C.01; Gaussian, Inc.: Wallingford, CT, 2004.
- (41) Morrow, T. L.; Maginn, E. J. *J. Phys. Chem. B* **2002**, *106*, 12807.
- (42) Logothetis, G.-E.; Ramos, J.; Economou, I. G. *J. Phys. Chem. B* **2009**, *113*, 7211.
- (43) Zhong, X.; Liu, Z.; Cao, D. *J. Phys. Chem. B* **2011**, *115*, 10027.
- (44) Youngs, T. G. A.; Hardacre, C. *ChemPhysChem* **2008**, *9*, 1548.
- (45) Wendler, K.; Dommer, F.; Zhao, Y. Y.; Berger, R.; Holm, C.; Delle Site, L. *Faraday Discuss.* **2011**, *154*, 1.
- (46) Huddleston, J. G.; Visser, A. E.; Reichert, W. M.; Willauer, H. D.; Broker, G. A.; Rogers, R. D. *Green Chem.* **2001**, *3*, 156–164.
- (47) Batista, M. L. S.; Neves, C. M. S. S.; Tomé, L. I.; Gomes, J. R. B.; Coutinho, J. A. P. Unpublished results.
- (48) Esperanca, J.; Lopes, J. N. C.; Tariq, M.; Santos, L.; Magee, J. W.; Rebelo, L. P. N. *J. Chem. Eng. Data* **2010**, *55*, 3–12.
- (49) Domanska, U.; Laskowska, M. *J. Chem. Eng. Data* **2009**, *54*, 2113–2119.
- (50) Marcinak, A. *Int. J. Mol. Sci.* **2010**, *11*, 1973–1990.
- (51) Freire, M. G.; Neves, C. M. S. S.; Silva, A. M. S.; Santos, L. M. N. B. F.; Marrucho, I. M.; Rebelo, L. P. N.; Shah, J. K.; Maginn, E. J.; Coutinho, J. A. P. *J. Phys. Chem. B* **2010**, *114*, 2004–2014.
- (52) Freire, M. G.; Carvalho, P. J.; Silva, A. M. S.; Santos, L. M. N. B. F.; Rebelo, L. P. N.; Marrucho, I. M.; Coutinho, J. A. P. *J. Phys. Chem. B* **2009**, *113*, 202–211.